nature geoscience

ARTICLES

https://doi.org/10.1038/s41561-017-0006-3

Oxygenation as a driver of the Great Ordovician Biodiversification Event

Cole T. Edwards[1]*, Matthew R. Saltzman[2], Dana L. Royer[3] and David A. Fike[4]

The largest radiation of Phanerozoic marine animal life quadrupled genus-level diversity towards the end of the Ordovician Period about 450 million years ago. A leading hypothesis for this Great Ordovician Biodiversification Event is that cooling of the Ordovician climate lowered sea surface temperatures into the thermal tolerance window of many animal groups, such as corals. A complementary role for oxygenation of subsurface environments has been inferred based on the increasing abundance of skeletal carbonate, but direct constraints on atmospheric O_2 levels remain elusive. Here, we use high-resolution paired bulk carbonate and organic carbon isotope records to determine the changes in isotopic fractionation between these phases throughout the Ordovician radiation. These results can be used to reconstruct atmospheric O_2 levels based on the O_2-dependent fractionation of carbon isotopes by photosynthesis. We find a strong temporal link between the Great Ordovician Biodiversification Event and rising O_2 concentrations, a pattern that is corroborated by O_2 models that use traditional carbon–sulfur mass balance. We conclude that that oxygen levels probably played an important role in regulating early Palaeozoic biodiversity levels, even after the Cambrian Explosion.

During the Ordovician period one of the greatest biological radiations of the Phanerozoic took place, when genus-level diversity quadrupled and ecospace utilization increased[1]. During this Great Ordovician Biodiversification Event (GOBE), marine communities expanded into new niches such as epifaunal suspension feeding and deep burrowing[2]. This new niche space was largely exploited by members of the Palaeozoic Evolutionary Fauna (EF), which includes articulated brachiopods, crinoids, ostracodes, cephalopods, corals, and bryozoans[1]. Both the Cambrian EF (trilobites and inarticulate brachiopods) and Modern EF (bivalves, gastropods, fish, and so on) also diversified, but it was the expansion of the Paleozoic EF that drove the GOBE.

The causes of the GOBE remain poorly understood and may include both intrinsic biological factors and external environmental drivers (such as global cooling, nutrient delivery from erosion, higher sea levels that expanded habitable platform area, and oxygenation)[1,3–5]. Oxygen isotopes from well-preserved conodont apatite provide proxy evidence for high sea surface temperatures (~40 °C) at the onset of the Ordovician that may have inhibited diversification, but global cooling throughout the Early–Middle Ordovician brought temperatures closer to modern conditions and possibly into the tolerance window (27–32 °C) for members of the Palaeozoic EF[6]. Cooling oceans could also store more dissolved oxygen and more effectively ventilate subsurface environments, which would in turn create a stronger vertical gradient in carbonate saturation that lowered the metabolic costs of skeletal carbonate biomineralization in surface waters[7]. A global increase in atmospheric oxygen[8] and oxygenation of shallow marine environments may have also eased stressful conditions for benthic animal life[9] and expanded the range of habitable ecospace for infaunal burrowers deeper into the sediment[10]. A more oxygenated ocean could also have supported more predators in the food chain (fish and cephalopods), setting into motion an evolutionary 'arms race'[11]. Ordovician global cooling is generally thought to have been caused by decreasing atmospheric CO_2 (the cause of this drop is itself not well understood, but hypotheses include increased silicate weathering[12] and the advent of land plants[13]), but a role for increased atmospheric O_2 is possible via an increase in total atmospheric pressure and the associated inhibition of solar optical depth, scattering incident solar radiation that would have otherwise contributed to the surface latent heat flux[14]. These arguments for linking oxygenation to cooling and biodiversification, while compelling, are hindered by poorly constrained ocean–atmosphere oxygen records. Existing isotope mass balance models are hampered by coarse time resolution (typically 10 Myr bins) that are not capable of resolving changes in atmospheric O_2 as a cause of the main pulses of biodiversification across the GOBE[15–17] (Supplementary Fig. 1). The absence of charcoal is interpreted to reflect atmospheric O_2 levels below 13–15% until the Late Silurian[18], but primitive non-vascular land plants only expanded into terrestrial environments by the Middle–Late Ordovician[13], thus the charcoal record is not well suited to constrain Early Ordovician O_2 levels. Land plant expansion is thought to have increased organic burial rates and oxygenated the atmosphere to near modern levels[13], but the timing and magnitude of this oxygenation is also poorly resolved. Similarly, although iron-based redox proxies suggest that O_2 levels were between 2% and 21% throughout the Ordovician, their resolution is not yet sufficient to resolve finer temporal trends[19]. Here we apply a new approach to reconstruct the changes in atmospheric oxygen with high age-resolution based on the O_2-dependence of carbon isotope fractionation during photosynthesis[20].

Effects of atmospheric O_2 on photosynthesis

Our estimates for Ordovician atmospheric O_2 are based on the link between photosynthetic fractionation of stable carbon isotopes in primary producers (such as marine phytoplankton) and changing O_2. The carbon fixation enzyme ribulose 1,5-bisphosphate carboxylase–oxygenase (Rubisco) has dual carboxylase/oxygenase functions, which results in variations in photosynthetic fractionation (ε_p) as a function of CO_2 and O_2 concentrations inside the cell[20–22]. Atmospheric O_2 in the past can thus be reconstructed if ε_p can be

[1]Department of Geological and Environmental Sciences, Appalachian State University, Boone, NC, USA. [2]School of Earth Sciences, The Ohio State University, Columbus, OH, USA. [3]Department of Earth and Environmental Sciences, Wesleyan University, Middletown, CT, USA. [4]Department of Earth and Planetary Sciences, Washington University in St. Louis, St. Louis, MO, USA. *e-mail: edwardsct4@appstate.edu

reasonably estimated and the influence of changing CO_2 concentrations on ε_p is accounted for.

We estimate ε_p from paired carbon isotopic measurements of carbonate rocks ($\delta^{13}C_{carb}$) and bulk organic matter ($\delta^{13}C_{org}$), which serve as proxies for the dissolved inorganic carbon (DIC) reservoir (δ_d) and average phytoplankton biomass (δ_p), respectively[23] (Fig. 1; Supplementary Table 2). These data come from a range of geologic settings, including the Great Basin (western United States), North American midcontinent, eastern North America and Anticosti Island (Canada), and Argentine Precordillera. Biases associated with gradients in seawater $\delta^{13}C$ or isolated populations of phytoplankton with site-specific algal growth rates or physiologies are minimized when compiled using data from a range of ocean basins and environments to highlight long-term trends. The estimated isotopic fractionation during photosynthesis in phytoplankton ($\varepsilon_{p\text{-estimated}}$) can be expressed as[24]:

$$\varepsilon_{p-estimated}(‰) = \left[(\delta_d + 1{,}000)/(\delta_p + 1{,}000) - 1\right] \times 1{,}000 \quad (1)$$

To estimate δ_d we adjust $\delta^{13}C_{carb}$ for fractionation effects associated with temperature (using estimates from the literature[6]) and the formation of carbonate in seawater (Supplementary Fig. 7; see Supplementary Information for calculations, a discussion of corrections, and sensitivity testing for constant and alternative temperature estimates). To estimate δ_p we adjust $\delta^{13}C_{org}$ to take into account the ^{13}C enrichment by secondary microbial heterotrophy on biomass (average + 1.5‰[25]). We recognize that deriving ε_p from bulk carbonate and organic matter is difficult considering that ε_p can be species-specific and influenced by algal physiology and growth rate[22], and that it is particularly challenging to estimate ε_p globally on geologic time scales. Comparison in other Paleozoic strata between $\delta^{13}C_{org}$ and its associated biomarker compounds, thought to be most representative of the original biomass, shows that bulk organic trends can faithfully preserve $\delta^{13}C$ trends of biomass[26,27] with the notable exception of highly productive coastal upwelling systems[28].

Although circulation patterns are poorly constrained for the epeiric sea from which a portion of the samples used in this study were collected, strong upwelling systems analogous to the modern Peruvian margin[28], if present, were probably confined to the western Laurentian continental margin[29]. Nonetheless, we consider our ε_p record a first-order approximation. The large number of paired $\delta^{13}C$ measurements used here ($n = 945$) permits the use of a locally weighted smoothing line (LOESS, $\alpha = 0.2$) to capture the overall trend in $\varepsilon_{p\text{-estimated}}$, which increased from about 20.2‰ during the Early Ordovician to 22.5‰ during the middle Late Ordovician (Supplementary Fig. 3).

It may be possible that this pattern of increasing ε_p is a function of biologic controls (such as variations in the dominant phytoplankton populations, productivity and growth rates, cell size) rather than environmental changes. This interval spans the 'Ordovician Plankton Revolution', a period recognized for the diversification of several plankton groups[30], but the poor fossil record of Ordovician phytoplankton (that is, acritarchs) makes it difficult to assess the true diversity of algae. However, considering that this overall ε_p increase occurred over several million years and is reproducible across several basins, we infer that local biologic factors were not as important as ambient CO_2 and O_2 levels, which are more likely to affect the carbon cycle globally. Thus, an increase in ε_p can best be explained by some combination of either rising atmospheric CO_2 or O_2 because both molecules directly impact isotopic fractionation during carbon fixation via Rubisco.

In experimental settings where it is possible to directly measure ε_p, the value expected for a given CO_2 change and set of growth conditions at fixed O_2 is calculated using the following relationship[21,22]:

$$\varepsilon_{p-expected}(‰) = \varepsilon_f - b/[CO_2]_{aq} \quad (2)$$

where ε_f is the maximum fractionation possible from photosynthesis (25‰), b is the sum of species-specific factors such as growth rate and cell geometry (we use the empirically derived value of $b = 171$ from ref. [31]; this approach assumes simple CO_2 diffusion into

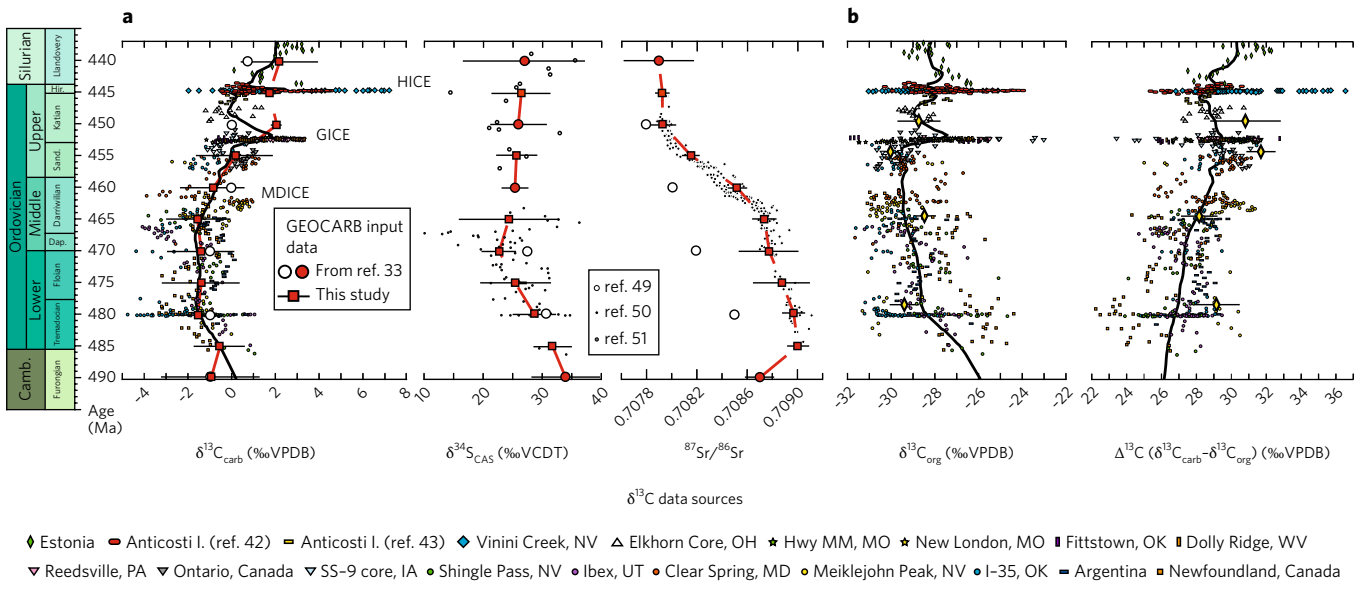

Fig. 1 | Isotope data used to model Ordovician atmospheric O_2 and CO_2. **a**, GEOCARB modelling results. **b**, Photosynthetic fractionation[56]. Data used to calculate mean values for 5 Myr time bins herein (red squares) with 2σ error bars are in good agreement with values used in the GEOCARB base model (large white circles, red circles used in standard run herein) (except $^{87}Sr/^{86}Sr$ data[57]). Black lines through $\delta^{13}C$ plots represent smoothed LOESS lines. Globally recognized $\delta^{13}C_{carb}$ excursions are indicated as the HICE, GICE, and MDICE (Middle Darriwilian). Yellow diamonds for $\delta^{13}C_{org}$ and $\Delta^{13}C$ show mean values and 2σ error bars[25].

the cell during periods with high CO_2 (for example, the Cretaceous and Ordovician) and excludes effects of carbon-concentrating mechanisms known from modern phytoplankton growing at low CO_2), and $[CO_2]_{aq}$ is the dissolved CO_2 concentration governed by Henry's law. We use new CO_2 results from the GEOCARBSULFvolc model[16,17,32] (referred to herein as GEOCARB) described below, which we update using high-resolution Ordovician $\delta^{13}C$, $\delta^{34}S$ and $^{87}Sr/^{86}Sr$ records (Fig. 1) to improve the model's ability to estimate time-resolved CO_2 to approximate $[CO_2]_{aq}$ and calculate $\varepsilon_{p\text{-expected}}$. This introduces a degree of non-independence between our two models, but independent CO_2 estimates from the COPSE model[13] yield similar O_2 results (Supplementary Fig. 4b).

If the variations in $\varepsilon_{p\text{-estimated}}$ (which is based on the difference between $\delta^{13}C_{carb}$ and $\delta^{13}C_{org}$) were solely caused by the changes in atmospheric CO_2 from GEOCARB, then $\varepsilon_{p\text{-expected}} = \varepsilon_{p\text{-estimated}}$. The $\varepsilon_{p\text{-expected}}$ trend (from GEOCARB CO_2) shows essentially no change between 22.1‰ to 22.5‰ throughout the Early–Middle Ordovician, and later decreases to 20.9‰ into the Late Ordovician (Supplementary Fig. 3). Values of $\varepsilon_{p\text{-estimated}}$ during the Early and early Middle Ordovician vary between 20.0‰ and 20.5‰ (average 20.2‰), but sharply increase to ~22.5‰ by the early Late Ordovician (Supplementary Fig. 3), which seems to be driven by the end of the long-term cooling trend during the Middle Ordovician[6] and the overall increase in the difference between $\delta^{13}C_{carb}$ and $\delta^{13}C_{org}$ ($\Delta^{13}C$; Fig. 1). This increase in $\varepsilon_{p\text{-estimated}}$ would then require CO_2 levels to have increased over this period, which is contrary to models that indicate CO_2 decreased steadily from >2,800 ppm during the Early Ordovician to <2,000 ppm during the Late Ordovician[13,15–17,33] (Supplementary Fig. 1). Thus we assume that the observed increase in $\varepsilon_{p\text{-estimated}}$ is instead caused by an increase in atmospheric O_2 (that is, controlled by the oxygenase function of Rubisco[20,34]). We also assume that factors such as cellular growth rates or cell size did not vary significantly on a regional scale to produce the observed increase in $\varepsilon_{p\text{-estimated}}$ in multiple basins simultaneously (see Supplementary Information). Whereas changes in marine phytoplankton cell size have been shown to have occurred in the past within specific algal assemblages[35], and considering that these biological factors affect ε_p individually and on a population scale, we presume here that the integration of bulk organic matter from separate ocean basins will minimize these biotic effects.

Modelling Ordovician atmospheric O_2. To relate $\varepsilon_{p\text{-estimated}}$ to atmospheric O_2 we use the empirical relationship[20]:

$$\varepsilon_{p-estimated}(‰) = \varepsilon_{p-expected} + J \times \left(\left(M_{O_2}/38\right) - 1\right) \quad (3)$$

where, $\varepsilon_{p\text{-expected}}$ is the value corrected for palaeo-CO_2 effects using GEOCARB while assuming a present-day O_2 concentration (21%) (equation (2)), $J = 5$ is a scaling coefficient (see Supplementary Information for discussion and sensitivity testing for other values of J), and $M_{O2}/38$ = the mass of atmospheric oxygen in the past (in 10^{18} mol) relative to the present day. Further sensitivity testing explores how constant CO_2 levels and other factors affect O_2 results (Supplementary Fig. 4b).

The resultant O_2 trend from the O_2-dependent photosynthetic fractionation effect (equation (3)) predicts relatively low atmospheric O_2 levels during the Early Ordovician that subsequently increased to modern levels (>20%) by the Late Ordovician. Although the $\delta^{13}C$ data were carefully selected from data sets that were not likely to be severely impacted during diagenesis[23], individual calculated O_2 values exhibit significant scatter between successive measurements (Supplementary Fig. 5). We run a LOESS smoothing line through the data with a 95% confidence interval envelope to capture the overall trend in O_2 (Fig. 2). Based on this smoothed trend, O_2 levels varied between 10% and 13% throughout the Early Ordovician and earliest Middle Ordovician and sharply rose throughout the Middle and early Late Ordovician to values as high as ~24% by the Katian. During the Hirnantian, a major O_2 decrease is observed that is coincident with the end-Ordovician mass extinction and glaciation, although artefacts related to uncertainty in the correlation of $\delta^{13}C$ data sets over this short time interval preclude in-depth interpretation[36] (Supplementary Fig. 6).

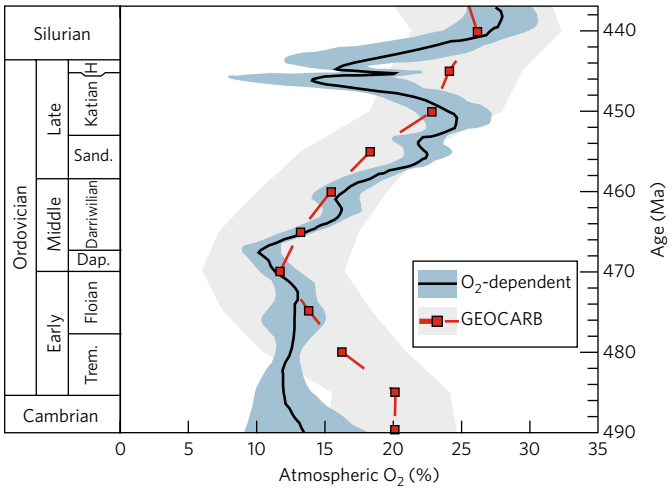

Fig. 2 | Model estimates of atmospheric O_2 using the GEOCARB and photosynthetic fractionation approaches. The dashed red line indicates the GEOCARB estimates, with the 2σ error envelope shaded in grey. The solid black line represents smoothed LOESS line of model results from the photosynthetic fractionation approach with 95% confidence interval of the overall trend shaded in blue (not the 2σ error envelope of each value). Both approaches indicate that atmospheric O_2 increased during the Darriwilian (Middle Ordovician) and continued to rise to near modern levels by the Katian (Late Ordovician).

We compare these new atmospheric O_2 results derived from O_2-dependent photosynthetic fractionation (equation (3)) with the component of the GEOCARB model that calculates O_2 using $\delta^{13}C$ and $\delta^{34}S$ data. We modified the published GEOCARB model[33] by incorporating both published and new high-resolution $\delta^{13}C$, $\delta^{34}S$, and $^{87}Sr/^{86}Sr$ data (Supplementary Tables 1 and 3). To increase the likelihood of resolving a possible relationship between the GOBE and O_2, we averaged these data into 5 Myr bins, increasing the typical resolution of the model by a factor of two (Fig. 1; Supplementary Table 1). We linearly interpolated all other time-dependent inputs for the new 5 Myr time step (appendix A in ref. [33]), which introduces some artificial smoothing. Following ref. [33], we constrained uncertainty of O_2 and CO_2 estimates by propagating uncertainties in all 68 input factors with Monte Carlo simulations (see Supplementary Information for a discussion on error analysis and error propagation using GEOCARB).

Our new Ordovician O_2 estimates using GEOCARB are broadly similar to previous GEOCARB results[33] with the important exception that our high-resolution data identify an O_2 increase during the Middle and Late Ordovician (Supplementary Fig. 1). Atmospheric O_2 estimates from both the photosynthetic fractionation (equation (3)) and geochemical models are largely in agreement with each other during Middle–Late Ordovician and indicate a rapid rise in atmospheric O_2 from ~14% during the Darriwilian (465–460 Ma (Ma)) to ~25% by the mid Katian (455–450 Ma) (Fig. 2). However, discrepancies between the two approaches occur during the Early Ordovician and Late Ordovician (Fig. 2). The relatively high O_2 estimates from GEOCARB during the Early Ordovician appear to contradict evidence for recurrent episodes of anoxic conditions that is

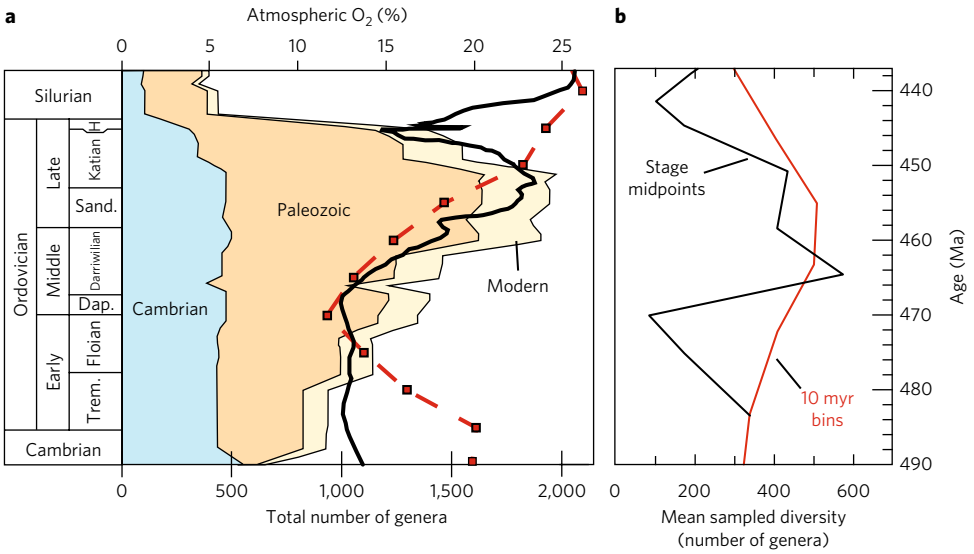

Fig. 3 | Long-term biodiversity curves. a, The total genera from the late Cambrian to early Silurian with the relative amounts of the three evolutionary faunas[1], overlain by modelled atmospheric O_2 trends from Fig. 2. Data from the Paleobiology Database (see Supplementary Information for details). **b**, Biodiversity trends using the Shareholder Quorum Subsampling normalization method[38] were made using the tools available at http://fossilworks.org.

based on palaeontological and geochemical data[9], which may reflect the spatial variability of anoxic conditions. In addition, because isotope mass balance models such as GEOCARB are sensitive to both $\delta^{13}C$ and $\delta^{34}S$, spatial heterogeneities that may have characterized the early Palaeozoic seawater sulfate reservoir (less than a third of the modern reservoir[37]) may explain differences between the two approaches for reconstructing O_2 at this time. For example, the $\delta^{34}S$ data used herein and in previous models[16,17,33] may not reflect the global sulfate reservoir, particularly if ocean circulation was sluggish or stratified under a warmer climate. Sensitivity testing of GEOCARB shows that the combination of $\delta^{13}C$ and $\delta^{34}S$ drives the observed O_2 patterns such that neither input alone is sufficient to generate the time-varying O_2 estimates (see Supplementary Information).

Effects of oxygenation on biodiversity. Ocean–atmosphere oxygenation during the Ordovician seems to be an important driver of long-term biodiversity trends (Fig. 3). Our updated generic biodiversity curve comes from the Paleobiology Database (see Supplementary Information for a discussion of data and error checking) where we account for variations in sampling intensity and collection size (that is, the 'monograph' effect) by normalizing taxonomic data using the Shareholder Quorum Subsampling method[38] at both stage midpoints and 10 Myr intervals (Fig. 3). Despite the coarse Myr-resolution of these standardized trends (the minimum available at present using http://fossilworks.org), the timing and overall trend of the GOBE is still clear and is similar to others that show brachiopods[39,40] and all taxa[1] rapidly increasing during the Middle Ordovician and peaking by the Late Ordovician (Supplementary Fig. 9). Taxa belonging to the Palaeozoic EF seem to be highly responsive to a more oxygenated ocean, as do the Modern and Cambrian EFs to a lesser extent. A post-Tremadocian (Early Ordovician) increase in the abundance of heavily skeletonized taxa is interpreted to reflect subsurface water mass oxygenation that increased carbonate saturation state in the overlying shallow marine settings[7]. It remains unclear whether increased O_2 also had a direct effect on animal life by permitting larger body plans and enhanced 'arms race' predator–prey relationships[8,11], or if it had a more passive effect by expanding the oxygenated ecospace of benthic environments[41]. A temperature control on biodiversification cannot be ruled out, as cooling oceans could store a greater concentration of dissolved O_2[6], thus making it difficult to resolve whether temperature or an associated increase in oxygen availability was the underlying driver of biodiversification.

The photosynthetic fractionation model suggests a 10% drop in atmospheric O_2 during the end-Ordovician (Fig. 2) that is not produced in the GEOCARB approach. This drop may be an artifact of: (1) large and rapid (<5 Myr) increases in CO_2 that are not captured in GEOCARB, (2) different age resolutions of the two data sets (5 Myr versus ~0.01 Myr) preventing high-frequency environmental change from being captured[37], or (3) age assignments of $\delta^{13}C$ from sections with poor biostratigraphic age control[42,43] that overemphasize the duration of low $\varepsilon_{p\text{-estimated}}$ values (that is, an O_2 drop) (Supplementary Fig. 6). Several lines of geochemical evidence[36,44] suggest that the Hirnantian records a period of oxygenation as oceans were progressively ventilated from ocean overturn during glaciation[45], with the cooling climate itself contributing to ocean oxygenation[46]. Future work specifically aimed at addressing the possibility of a Late Ordovician oxygen crisis is needed to resolve whether these model results capture a real signal.

The cause of this Middle Ordovician oxygenation is not well understood but its onset seems to be rooted in the late Cambrian, when deep sea anoxia gradually diminished[9]. The late Cambrian–Early Ordovician is known for high extinction rates linked to episodic upwelling of anoxic waters into surface oceans, which resulted in enhanced organic carbon and pyrite sulfur burial (inferred from positive $\delta^{13}C$ and $\delta^{34}S$ excursions, respectively)[9]. These extinction events and high-frequency positive $\delta^{13}C$ excursions abate before the first biodiversity pulses that comprise the GOBE. This may indicate that a threshold in subsurface water ventilation was reached that allowed O_2 to build up in the atmosphere and shallow surface ocean, locations that experienced faster O_2 exchange rates than those between the surface ocean and deeper anoxic bottom waters.

Methods

Methods, including statements of data availability and any associated accession codes and references, are available at https://doi.org/10.1038/s41561-017-0006-3.

Received: 29 May 2017; Accepted: 6 October 2017;
Published online: 20 November 2017

References

1. Sepkoski, J. J. J. The Ordovician radiations: diversification and extinction shown by global genus-level taxonomic data. In *Ordovician Odyssey Short Papers for the Seventh Int. Symp. on the Ordovician System* 393–396 (SEPM, 1995).
2. Webby, B. D., Paris, F., Droser, M. L. & Percival, I. G. *The Great Ordovician Biodiversification Event* (Columbia Univ. Press, 2004).
3. Servais, T., Owen, A. W., Harper, D. A. T., Kröger, B. & Munnecke, A. The Great Ordovician Biodiversification Event (GOBE): The palaeoecological dimension. *Palaeogeogr. Palaeoclimatol. Palaeoecol.* **294**, 99–119 (2010).
4. Miller, A. I. in *Earth and Life* (ed. Talent, J. A.) 381–394 (Springer, 2012).
5. Harper, D. A. T., Zhan, R.-B. & Jin, J. The Great Ordovician Biodiversification Event: Reviewing two decades of research on diversity's big bang illustrated by mainly brachiopod data. *Palaeoworld* **24**, 75–85 (2015).
6. Trotter, J. A., Williams, I. S., Barnes, C. R., Lécuyer, C. & Nicoll, R. S. Did cooling oceans trigger Ordovician biodiversification? Evidence from conodont thermometry. *Science* **321**, 550–554 (2008).
7. Pruss, S. B., Finnegan, S., Fischer, W. W. & Knoll, A. H. Carbonates in skeleton-poor seas: new insights from Cambrian and Ordovician strata of Laurentia. *Palaios* **25**, 73–84 (2010).
8. Berner, R. A., VandenBrooks, J. M. & Ward, P. D. Oxygen and evolution. *Science* **316**, 557–558 (2007).
9. Saltzman, M. R., Edwards, C. T., Adrain, J. M. & Westrop, S. R. Persistent oceanic anoxia and elevated extinction rates separate the Cambrian and Ordovician radiations. *Geology* **43**, 807–810 (2015).
10. Droser, M. L. & Bottjer, D. J. Trends and patterns of Phanerozoic ichnofabrics. *Annu. Rev. Earth Planet. Sci.* **21**, 205–225 (1993).
11. Sperling, E. A. et al. Oxygen, ecology, and the Cambrian radiation of animals. *Proc. Natl Acad. Sci. USA* **110**, 13446–51 (2013).
12. Swanson-Hysell, N. L. & Macdonald, F. A. Tropical weathering of the Taconic orogeny as a driver for Ordovician cooling. *Geology* **45**, 719–725 (2017).
13. Lenton, T. M. et al. Earliest land plants created modern levels of atmospheric oxygen. *Proc. Natl Acad. Sci. USA* **113**, 9704–9709 (2016).
14. Poulsen, C. J., Tabor, C. & White, J. D. Atmospheric oxygen concentrations. *Science* **348**, 1238–1242 (2015).
15. Bergman, N. M., Lenton, T. M. & Watson, A. J. COPSE: A new model of biogeochemical cycling over Phanerozoic time. *Am. J. Sci.* **304**, 397–437 (2004).
16. Berner, R. A. GEOCARBSULF: A combined model for Phanerozoic atmospheric O_2 and CO_2. *Geochim. Cosmochim. Acta* **70**, 5653–5664 (2006).
17. Berner, R. A. Phanerozoic atmospheric oxygen: new results using the GEOCARBSULF model. *Am. J. Sci.* **309**, 603–606 (2009).
18. Algeo, T. J. & Ingall, E. Sedimentary C_{org}:P ratios, paleocean ventilation, and Phanerozoic atmospheric pO_2. *Palaeogeogr. Palaeoclimatol. Palaeoecol.* **256**, 130–155 (2007).
19. Sperling, E. A. et al. Statistical analysis of iron geochemical data suggests limited late Proterozoic oxygenation. *Nature* **523**, 451–454 (2015).
20. Berner, R. A. et al. Isotope fractionation and atmospheric oxygen: Implications for phanerozoic O_2 evolution. *Science* **287**, 1630–1633 (2000).
21. Bidigare, R. R. et al. Consistent fractionation of ^{13}C in nature and in the laboratory: growth-rate effects in some haptophyte algae. *Glob. Biogeochem. Cycles* **11**, 279–292 (1997).
22. Popp, B. N. et al. Effect of phytoplankton cell geometry on carbon isotopic fractionation. *Geochim. Cosmochim. Acta* **62**, 69–77 (1998).
23. Edwards, C. T. & Saltzman, M. R. Paired carbon isotopic analysis of Ordovician bulk carbonate ($\delta^{13}C_{carb}$) and organic matter ($\delta^{13}C_{org}$) spanning the Great Ordovician Biodiversification Event. *Palaeogeogr. Palaeoclimatol. Palaeoecol.* **458**, 102–117 (2016).
24. Freeman, K. H. & Hayes, J. M. Fractionation of carbon isotopes by phytoplankton and estimates of ancient CO_2 levels. *Glob. Biogeochem. Cycles* **6**, 185–198 (1992).
25. Hayes, J. M., Strauss, H. & Kaufman, A. J. The abundance of in marine organic matter and isotopic fractionation in the global biogeochemical cycle of carbon during the past 800 Ma. *Chem. Geol.* **161**, 103–125 (1999).
26. Pancost, R. D. et al. Reconstructing Late Ordovician carbon cycle variations. *Geochim. Cosmochim. Acta* **105**, 433–454 (2013).
27. Joachimski, M. M., Pancost, R. D., Freeman, K. H., Ostertag-Henning, C. & Buggisch, W. Carbon isotope geochemistry of the Frasnian–Famennian transition. *Palaeogeogr. Palaeoclimatol. Palaeoecol.* **181**, 91–109 (2002).
28. Pancost, R. D., Freeman, K. H. & Wakeham, S. G. Controls on the carbon-isotope compositions of compounds in Peru surface waters. *Org. Geochem.* **30**, 319–340 (1999).
29. Pope, M. C. & Steffen, J. B. Widespread, prolonged late Middle to Late Ordovician upwelling in North America: a proxy record of glaciation? *Geology* **31**, 63–66 (2003).
30. Servais, T. et al. The onset of the "Ordovician Plankton Revolution" in the late Cambrian. *Palaeogeogr. Palaeoclimatol. Palaeoecol.* **458**, 12–28 (2016).
31. Naafs, B. D. A. et al. Gradual and sustained carbon dioxide release during Aptian Oceanic Anoxic Event 1a. *Nat. Geosci.* 135–139 (2016).
32. Berner, R. A. Inclusion of the weathering of volcanic rocks in the GEOCARBSULF model. *Am. J. Sci.* **306**, 295–302 (2006).
33. Royer, D. L., Donnadieu, Y., Park, J., Kowalczyk, J. & Goddéris, Y. Error analysis of CO_2 and O_2 estimates from the long-term geochemical model GEOCARBSULF. *Am. J. Sci.* **314**, 1259–1283 (2014).
34. Beerling, D. J. et al. The influence of Carboniferous palaeo-atmospheres on plant function: an experimental and modelling assessment. *Phil. Trans. R. Soc. B* **353**, 131–140 (1998).
35. Henderiks, J. & Pagani, M. Coccolithophore cell size and the Paleogene decline in atmospheric CO_2. *Earth Planet. Sci. Lett.* **269**, 575–583 (2008).
36. Melchin, M. J., Mitchell, C. E., Holmden, C. & Štorch, P. Environmental changes in the Late Ordovician–early Silurian: Review and new insights from black shales and nitrogen isotopes. *Geol. Soc. Am. Bull.* **125**, 1635–1670 (2013).
37. Jones, D. S. & Fike, D. A. Dynamic sulfur and carbon cycling through the end-Ordovician extinction revealed by paired sulfate–pyrite $\delta^{34}S$. *Earth Planet. Sci. Lett.* **363**, 144–155 (2013).
38. Alroy, J. Accurate and precise estimates of origination and extinction rates. *Paleobiology* **40**, 374–397 (2014).
39. Harper, D. A. T. et al. Biodiversity, biogeography and phylogeography of Ordovician rhynchonelliform brachiopods. *Mem. Geol. Soc. Lond.* **38**, 127–144 (2013).
40. Trubovitz, S. & Stigall, A. L. Synchronous diversification of Laurentian and Baltic rhynchonelliform brachiopods: Implications for regional versus global triggers of the Great Ordovician Biodiversification Event. *Geology* **44**, 743–746 (2016).
41. Graham, J. B., Dudley, R., Aguilar, N. M. & Gans, C. Implications of the late Palaeozoic oxygen pulse for physiology and evolution. *Nature* **375**, 117–120 (1995).
42. Young, S. A., Saltzman, M. R., Ausich, W. I., Desrochers, A. & Kaljo, D. Did changes in atmospheric CO_2 coincide with latest Ordovician glacial-interglacial cycles? *Palaeogeogr. Palaeoclimatol. Palaeoecol.* **296**, 376–388 (2010).
43. Jones, D. S. et al. Terminal Ordovician carbon isotope stratigraphy and glacioeustatic sea-level change across Anticosti Island (Québec, Canada). *Geol. Soc. Am. Bull.* **123**, 1645–1664 (2011).
44. Rohrssen, M., Love, G. D., Fischer, W., Finnegan, S. & Fike, D. A. Lipid biomarkers record fundamental changes in the microbial community structure of tropical seas during the Late Ordovician Hirnantian glaciation. *Geology* **41**, 127–130 (2013).
45. Brenchley, P. J., Carden, G. A. F. & Marshall, J. D. Environmental changes assoicated with the "first strike" of the Late Ordovician mass extinction. *Mod. Geol.* **20**, 69–82 (1995).
46. Pohl, A., Donnadieu, Y., Le Hir, G. & Ferreira, D. The climatic significance of Late Ordovician-early Silurian black shales. *Paleoceanography* **32**, 397–423 (2017).
56. Kampschulte, A. & Strauss, H. The sulfur isotopic evolution of Phanerozoic seawater based on the analysis of structurally substituted sulfate in carbonates. *Chem. Geol.* **204**, 255–286 (2004).
57. Saltzman, M. R. et al. Calibration of a conodont apatite-based Ordovician $^{87}Sr/^{86}Sr$ curve to biostratigraphy and geochronology: Implications for stratigraphic resolution. *Bull. Geol. Soc. Am.* **126**, 1551–1568 (2014).

Acknowledgements

J. Houghton is thanked for valuable discussions in improving earlier versions of this paper. This paper is a contribution to IGCP Projects 591 and 653. Funding was provided in part by the Evolving Earth Foundation (CTE), a Geological Society of America Graduate Student Research Grant (CTE), a Paleontological Society Student Research Grant (CTE) and NSF Grants EAR-0819832 and EAR-0745452 (M.R.S.).

Author contributions

This project was conceived by C.T.E. and M.R.S. with input from D.L.R. and D.A.F. Isotopic data preparation and analysis was done by C.T.E. Modelling was conducted by C.T.E. with input from D.L.R. The manuscript was developed by C.T.E. and received equal contributions from all authors on editing the final manuscript.

Competing interests

The authors declare no competing financial interests.

Additional information

Supplementary information is available for this paper at https://doi.org/10.1038/s41561-017-0006-3.

Reprints and permissions information is available at www.nature.com/reprints.

Correspondence and requests for materials should be addressed to C.T.E.

Publisher's note: Springer Nature remains neutral with regard to jurisdictional claims in published maps and institutional affiliations.

Methods

Geochemistry. New $\delta^{13}C_{org}$ data presented here were measured from samples previously measured for $\delta^{13}C_{carb}$ from the Elkhorn Core of western Ohio[47]. Core samples were crushed and powdered using a mortar and pestle to produce about 1–2 g of powdered carbonate. Samples were acidified using 10 ml of 3 M HCl and centrifuged to decant off spent acid. This step was repeated twice (three in total), followed by three rinses with 10 ml of distilled water and centrifuge. Acidified insoluble residues were dried, homogenized and weighed out into tin capsules for isotopic analysis. Samples were analysed for $\delta^{13}C_{org}$ using a Costech ECS4010 Elemental Analyzer and passed to a ThermoFinnigan Delta V Plus mass spectrometer using a helium carrier gas via ConFlo IV at Washington University in St. Louis. Isotopic ratios are reported in delta notation (‰) relative to the Vienna Pee Dee Belemnite (VPDB) standard. The precision and calibration of data were monitored through routine analysis of internal and international standards. Standard deviations for $\delta^{13}C_{org}$ data are all less than 0.22‰.

Previously published data. Carbon isotopic data sets were selected based on reporting of paired $\delta^{13}C_{carb}$ and $\delta^{13}C_{org}$ measurements and overlapping coverage with each other of the entire Ordovician period. Data were also selected based on the temporal coverage of each study (generally longer than two or three conodont biozones) to improve our ability to assign age estimates for isotopic data. Although we selected studies with some overlap with each other, some time intervals of the Ordovician have received more attention for their globally correlative positive $\delta^{13}C$ excursions (for example, the Hirnantian and Guttenberg $\delta^{13}C$ excursions events (HICE and GICE, respectively)). These intervals are biased with respect to their $\delta^{13}C$ resolution compared with elsewhere in the Ordovician (the Floian stage, for example), but differences with respect to data density are minimized for GEOCARB estimates because each time step uses the average $\delta^{13}C$ value and variance for a given 5 Myr interval.

The paired $\delta^{13}C_{carb}$ and $\delta^{13}C_{org}$ data used in the modelling of this study come from: the Ikla Core, Estonia[48]; Vinini Creek, NV[49]; Dolly Ridge, WV and Fittstown, OK[50]; Argentina[51]; Newfoundland, Canada[52]; Anticosti Island, Canada[42,43]; SS-9 Core, IA, Reedsville, PA, and Ontario, Canada[26,53]; Highway MM and New London sections, Missouri[54]; Clear Spring, MD, Meiklejohn Peak, NV, Shingle Pass, NV, Ibex area, UT, Interstate-35 section, OK[23]; $\delta^{13}C_{carb}$ data from the Elkhorn Core, OH[47], and $\delta^{13}C_{org}$ data (this study). Sulfur isotope data come from Shingle Pass[55] and a compilation of samples throughout Middle–Upper Ordovician carbonates[56]. Strontium isotopic data come from a recent conodont-based $^{87}Sr/^{86}Sr$ compilation[57].

Code availability. The code used to generate the GEOCARB model results can be accessed at https://figshare.com/articles/code_to_run_GEOCARBSULF_model/902207.

Data availability. The authors declare that data supporting the findings of this study are available within the article and Supplementary Tables 1–4. The data used to construct biodiversity trends are available from Fossilworks at http://fossilworks.org.

References

47. Bergström, S. M., Young, S. & Schmitz, B. Katian (Upper Ordovician) $\delta^{13}C$ chemostratigraphy and sequence stratigraphy in the United States and Baltoscandia: A regional comparison. *Palaeogeogr. Palaeoclimatol. Palaeoecol.* **296**, 217–234 (2010).
48. Gouldey, J. C., Saltzman, M. R., Young, S. A. & Kaljo, D. Strontium and carbon isotope stratigraphy of the Llandovery (Early Silurian): Implications for tectonics and weathering. *Palaeogeogr. Palaeoclimatol. Palaeoecol.* **296**, 264–275 (2010).
49. Laporte, D. F. et al. Local and global perspectives on carbon and nitrogen cycling during the Hirnantian glaciation. *Palaeogeogr. Palaeoclimatol. Palaeoecol.* **276**, 182–195 (2009).
50. Young, S. A., Saltzman, M. R., Bergström, S. M., Leslie, S. A. & Xu, C. Paired $\delta^{13}C_{carb}$ and $\delta^{13}C_{org}$ records of Upper Ordovician (Sandbian–Katian) carbonates in North America and China: Implications for paleoceanographic change. *Palaeogeogr. Palaeoclimatol. Palaeoecol.* **270**, 166–178 (2008).
51. Buggisch, W., Keller, M. & Lehnert, O. Carbon isotope record of Late Cambrian to Early Ordovician carbonates of the Argentine Precordillera. *Palaeogeogr. Palaeoclimatol. Palaeoecol.* **195**, 357–373 (2003).
52. Azmy, K. & Lavoie, D. High-resolution isotope stratigraphy of the Lower Ordovician St. George Group of western Newfoundland, Canada: Implications for global correlation. *Can. J. Earth Sci.* **423**, 403–423 (2009).
53. Pancost, R. D., Freeman, K. H. & Patzkowsky, M. E. Organic-matter source variation and the expression of a late Middle Ordovician carbon isotope excursion. *Geology* **27**, 1015–1018 (1999).
54. Metzger, J. G. & Fike, D. A. Techniques for assessing spatial heterogeneity of carbonate $\delta^{13}C$ values: Implications for craton-wide isotope gradients. *Sedimentology* **60**, 1405–1431 (2013).
55. Edwards, C. T. *Carbon, Sulfur, and Strontium Isotope Stratigraphy of the Lower-Middle Ordovician, Great Basin, USA: Implications for Oxygenation andCauses of Global Biodiversification*. PhD thesis, Ohio State Univ. (2014).